Supplementary information for "Microrheology of Active Suspensions"

A Explicit time-integration algorithm

Here, following the references[1–3], we describe an explicit time-integration scheme for solving model equations as follows. The set of physical variables is assumed to be clearly defined at the discrete time step $t_n = n\Delta t$.

First, we solve Eq. (5) in the main text without including $\boldsymbol{f}_H$ as

$$\boldsymbol{v}^* = \boldsymbol{v}_n + \frac{1}{\rho}\int_{t_n}^{t_{n+1}} \mathrm{d}s\left(-\rho\boldsymbol{v}\cdot\boldsymbol{\nabla}\boldsymbol{v} + \boldsymbol{\nabla}\cdot\overleftrightarrow{\boldsymbol{\Sigma}}_{vis} + \boldsymbol{f}_A^{(f)}\right)^{\perp}, \tag{S1}$$

where $\boldsymbol{v}_n$ is the velocity field at $t = t_n$ and $(\cdots)^{\perp}$ denotes taking the transverse part.

Second, we update $\boldsymbol{R}_\alpha^{(G)}$, $\hat{\boldsymbol{n}}_\alpha$, and $\boldsymbol{R}_p$ as

$$\boldsymbol{R}_\alpha^{(G)}(t_{n+1}) = \boldsymbol{R}_\alpha^{(G)}(t_n) + \int_{t_n}^{t_{n+1}} \mathrm{d}s\boldsymbol{V}_\alpha^{(G)}, \tag{S2}$$

$$\hat{\boldsymbol{n}}_\alpha(t_{n+1}) = \hat{\boldsymbol{n}}_\alpha(t_n) + \int_{t_n}^{t_{n+1}} \mathrm{d}s\boldsymbol{\Omega}_\alpha^{(G)}\times\hat{\boldsymbol{n}}_\alpha, \tag{S3}$$

$$\boldsymbol{R}_p(t_{n+1}) = \boldsymbol{R}_p(t_n) + \int_{t_n}^{t_{n+1}} \mathrm{d}s\boldsymbol{V}_p. \tag{S4}$$

With these updated $\boldsymbol{R}_\alpha^{(G)}$, $\hat{\boldsymbol{n}}_\alpha$, and $\boldsymbol{R}_p$, we also update $\Psi_\alpha^{(b)}(\boldsymbol{r})$, $\Psi_\alpha^{(f)}(\boldsymbol{r})$, and $\Psi_p(\boldsymbol{r})$.

Third, the particle velocities and angular velocities are updated by solving Eqs. (9), (10), (16), and (17) in the main text as

$$\boldsymbol{V}_\alpha^{(G)}(t_{n+1}) = \boldsymbol{V}_\alpha^{(G)}(t_n) + \frac{1}{M_\alpha}\int_{t_n}^{t_{n+1}} \mathrm{d}s(\boldsymbol{F}_{\alpha,H} + \boldsymbol{F}_{\alpha,int} + \boldsymbol{F}_{\alpha,A}^{(b)}), \tag{S5}$$

$$\boldsymbol{\Omega}_\alpha^{(G)}(t_{n+1}) = \boldsymbol{\Omega}_\alpha^{(G)}(t_n) + \overleftrightarrow{\boldsymbol{I}}_\alpha^{-1}\cdot\left[\int_{t_n}^{t_{n+1}} \mathrm{d}s(\boldsymbol{N}_{\alpha,H} + \boldsymbol{N}_{\alpha,int})\right], \tag{S6}$$

$$\boldsymbol{V}_p(t_{n+1}) = \boldsymbol{V}_p(t_n) + \frac{1}{M_p}\int_{t_n}^{t_{n+1}} \mathrm{d}s(\boldsymbol{F}_{p,H} + \boldsymbol{F}_{p,int} + F_{ex}\hat{\boldsymbol{x}}), \tag{S7}$$

$$\boldsymbol{\Omega}_p(t_{n+1}) = \boldsymbol{\Omega}_p(t_n) + \frac{1}{I_p}\int_{t_n}^{t_{n+1}} \mathrm{d}s\boldsymbol{N}_{p,H}. \tag{S8}$$

Here, the explicit forms of $\int_{t_n}^{t_{n+1}} \mathrm{d}s\boldsymbol{F}_{\alpha,H}$, $\int_{t_n}^{t_{n+1}} \mathrm{d}s\boldsymbol{N}_{\alpha,H}$, $\int_{t_n}^{t_{n+1}} \mathrm{d}s\boldsymbol{F}_{p,H}$, and $\int_{t_n}^{t_{n+1}} \mathrm{d}s\boldsymbol{N}_{p,H}$ are given as

$$\int_{t_n}^{t_{n+1}} \mathrm{d}s\boldsymbol{F}_{\alpha,H} = \int \mathrm{d}\boldsymbol{r}\rho\Psi_{\alpha,n+1}^{(b)}\left\{\boldsymbol{v}^* - \left[\boldsymbol{V}_\alpha^{(G)}(t_n) + \boldsymbol{\Omega}_\alpha^{(G)}(t_n)\times\left(\boldsymbol{r} - \boldsymbol{R}_\alpha^{(G)}(t_{n+1})\right)\right]\right\}, \tag{S9}$$

$$\int_{t_n}^{t_{n+1}} \mathrm{d}s\boldsymbol{N}_{\alpha,H} = \int \mathrm{d}\boldsymbol{r}\rho\Psi_{\alpha,n+1}^{(b)}\left(\boldsymbol{r} - \boldsymbol{R}_\alpha^{(G)}(t_{n+1})\right)\times\left\{\boldsymbol{v}^* - \left[\boldsymbol{V}_\alpha^{(G)}(t_n) + \boldsymbol{\Omega}_\alpha^{(G)}(t_n)\times\left(\boldsymbol{r} - \boldsymbol{R}_\alpha^{(G)}(t_{n+1})\right)\right]\right\}, \tag{S10}$$

$$\int_{t_n}^{t_{n+1}} \mathrm{d}s\boldsymbol{F}_{p,H} = \int \mathrm{d}\boldsymbol{r}\rho\Psi_{p,n+1}\left\{\boldsymbol{v}^* - \left[\boldsymbol{V}_p(t_n) + \boldsymbol{\Omega}_p(t_n)\times\left(\boldsymbol{r} - \boldsymbol{R}_p(t_{n+1})\right)\right]\right\}, \tag{S11}$$

and

$$\int_{t_n}^{t_{n+1}} \mathrm{d}s\boldsymbol{N}_{p,H} = \int \mathrm{d}\boldsymbol{r}\rho\Psi_{p,n+1}\left(\boldsymbol{r} - \boldsymbol{R}_p(t_{n+1})\right)\times\left\{\boldsymbol{v}^* - \left[\boldsymbol{V}_p(t_n) + \boldsymbol{\Omega}_p(t_n)\times\left(\boldsymbol{r} - \boldsymbol{R}_p(t_{n+1})\right)\right]\right\}, \tag{S12}$$

where $\Psi_{\alpha,n+1}^{(b)}$ and $\Psi_{p,n+1}$ denote $\Psi_\alpha^{(b)}(\boldsymbol{r})$ and $\Psi_p(\boldsymbol{r})$ at $t = t_{n+1}$, respectively.

Finally, we update the velocity field by embedding the rigid body motions in $\boldsymbol{v}^*$ through the body force $\boldsymbol{f}_H$ as

$$\boldsymbol{v}_{n+1} = \boldsymbol{v}^* + \frac{1}{\rho}\int_{t_n}^{t_{n+1}} \mathrm{d}s\boldsymbol{f}_H^{\perp}. \tag{S13}$$

The explicit form of $\int_{t_n}^{t_{n+1}} \mathrm{d}s\boldsymbol{f}_H$ is determined to approximately fulfill the rigid body condition inside the regions of the swimmer bodies and the probe particle, and it is given by

$$\begin{aligned}\int_{t_n}^{t_{n+1}} \mathrm{d}s\boldsymbol{f}_H &= -\sum_{\alpha=1}^{N}\rho\Psi_{\alpha,n+1}^{(b)}\Big\{\boldsymbol{v}^* - \Big[\boldsymbol{V}_\alpha^{(G)}(t_{n+1}) + \boldsymbol{\Omega}_\alpha^{(G)}(t_{n+1})\times\big(\boldsymbol{r}-\boldsymbol{R}_\alpha^{(G)}(t_{n+1})\big)\Big]\Big\} \\ &\quad -\rho\Psi_{p,n+1}\Big\{\boldsymbol{v}^* - \Big[\boldsymbol{V}_p(t_{n+1}) + \boldsymbol{\Omega}_p(t_{n+1})\times\big(\boldsymbol{r}-\boldsymbol{R}_p(t_{n+1})\big)\Big]\Big\}. \end{aligned} \tag{S14}$$

Equations (S9)-(S12), and (S14) enforce the momentum and angular momentum exchanges between the solvent and swimmer bodies. The velocity field at the new time step is

$$\begin{aligned}\boldsymbol{v}_{n+1} = \boldsymbol{v}^*\big[1-\sum_{\alpha=1}^{N}\Psi_{\alpha,n+1}^{(b)} - \Psi_{p,n+1}\big] + \sum_{\alpha=1}^{N}\Psi_{\alpha,n+1}^{(b)}\Big[\boldsymbol{V}_\alpha^{(G)}(t_{n+1}) + \boldsymbol{\Omega}_\alpha^{(G)}(t_{n+1})\times\big(\boldsymbol{r}-\boldsymbol{R}_\alpha^{(G)}(t_{n+1})\big)\Big] \\ +\Psi_{p,n+1}\Big[\boldsymbol{V}_p(t_{n+1}) + \boldsymbol{\Omega}_p(t_{n+1})\times\big(\boldsymbol{r}-\boldsymbol{R}_p(t_{n+1})\big)\Big]\end{aligned} \tag{S15}$$

with

$$\nabla\cdot\boldsymbol{v}_{n+1} = 0. \tag{S16}$$

B Supporting simulations investigating front-rear asymmetry in scattering of swimmers

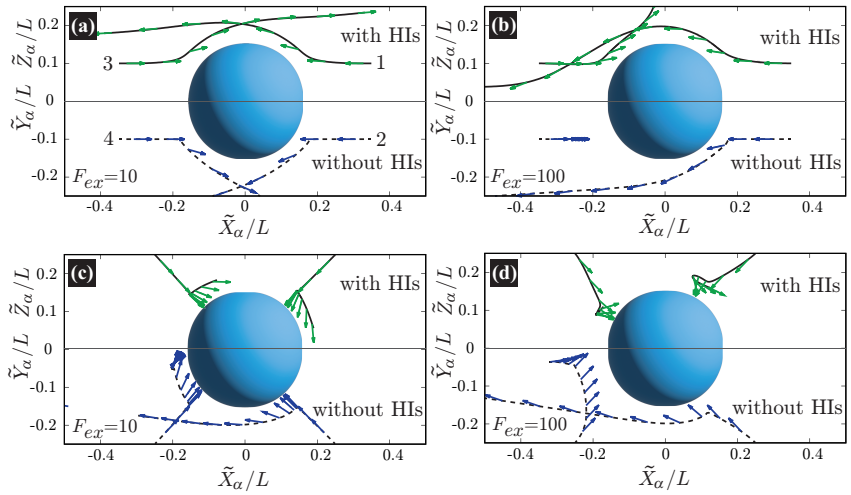

Fig. S1 (Color online) The trajectories of swimmers measured in the co-moving frame with the probe particle, $\boldsymbol{R}_\alpha^{(G)} - \boldsymbol{R}_p = (\tilde{X}_\alpha, \tilde{Y}_\alpha, \tilde{Z}_\alpha)$, are plotted. In (a) and (b), for $F_{ex} = 10$ and 100, respectively, swimmers 1 and 2 are initially placed at $\boldsymbol{R}_\alpha^{(G)} = (14a, \pm 4a, 0)$ with $\hat{\boldsymbol{n}}_\alpha = (-1, 0, 0)$, while swimmers 3 and 4 are at $\boldsymbol{R}_\alpha^{(G)} = (-14a, 0, \pm 4a)$ with $\hat{\boldsymbol{n}}_\alpha = (1, 0, 0)$. On the other hand, in (c) and (d), for $F_{ex} = 10$ and 100, respectively, swimmers 1 and 2 are initially placed at $\boldsymbol{R}_\alpha^{(G)} = (10a, \pm 10a, 0)$ with $\hat{\boldsymbol{n}}_\alpha = (-\sqrt{2}/2, \mp\sqrt{2}/2, 0)$, while swimmers 3 and 4 are at $\boldsymbol{R}_\alpha^{(G)} = (-10a, 0, \pm 10a)$ with $\hat{\boldsymbol{n}}_\alpha = (\sqrt{2}/2, 0, \mp\sqrt{2}/2)$. In (a)-(d), for swimmers 1 and 2, $(\tilde{X}_\alpha/L, \tilde{Y}_\alpha/L)$ is ploted, while for swimmers 3 and 4, $(\tilde{X}_\alpha/L, \tilde{Z}_\alpha/L)$ is ploted. By considering the spatial symmetry of the swimmer trajectories, the trajectories of swimmers 1 and 3 for the cases with HIs are plotted, and those of swimmers 2 and 4 for the cases without HIs are plotted. Furthermore, the arrows indicate the instantaneous directions of each swimmer.

The orientation distribution of swimmers $P(\hat{\theta}; x, y)$, shown in Fig. 5 in the main text, indicates that swimmers suffer from more significant scatterings at the front side than at the rear, resulting in the asymmetric shape of $P(\hat{\theta}; x, y)$ between the front and rear sides. Here, we present complementary simulation results, demonstrating front-rear asymmetry in scattering of swimmers with the following setup. At $t = 0$, the probe particle is placed at the center of the system, and four swimmers, with active force being turned off ($F_A = 0$), are arranged to face the probe in a spatially symmetric manner: swimmers 1 and 2 are on the front side and swimmers 3 and 4 are on the rear side, as illustrated in Fig. S1. For $t > 0$, the probe particle is dragged by a constant force (F_{ex}) along the x-direction, and the active force is turned on ($F_A = 20$). Then, these four swimmers move toward the probe from different directions.

The swimmer trajectories are shown in Fig. S1, demonstrating that the collision conditions and the presence or absence of HIs strongly influence the trajectories. With HIs, swimmers approaching the probe particle from the rear tend to face the probe more than those approaching from the front. This behavior is attributed to the comparatively weaker repulsive nature of HIs between swimmers

and the probe on the rear side than on the front. This repulsion on the rear side even becomes an attraction for larger values of F_{ex}. In contrast, without HIs, swimmers that collide with the probe from the front experience stronger repulsions than those approaching from the rear. Furthermore, as F_{ex} increases, swimmers from the rear cannot keep pace with those in the front.

C Orientation distributions of swimmers without HIs at $F_{ex} = 100$

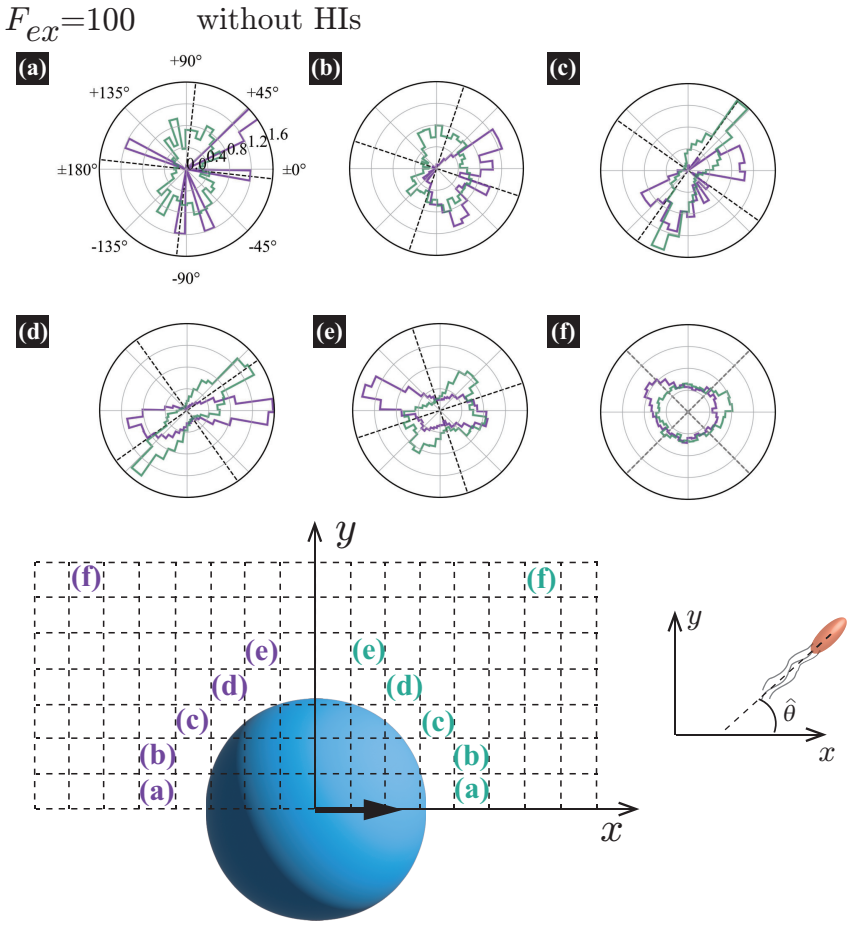

Fig. S2 (Color online) The orientation distributions of swimmers $P(\hat{\theta}; x, y)$ at $R = 20$, $\phi = 0.032$, and $F_{ex} = 100$ without HIs, with the block size being $2a = 0.32R(= 6.4)$. As described in the main text, $P(\hat{\theta}; x, y)$ is defined as $P(\hat{\theta}; x, y) = c(x, y) \sum_\alpha \langle \delta[\theta - \cos^{-1}(\hat{\boldsymbol{t}}_\alpha \cdot \hat{\boldsymbol{x}})] \delta(\boldsymbol{r} - \boldsymbol{R}_\alpha) \rangle$, where $\boldsymbol{r} = (x, y, 0)$, $\hat{\boldsymbol{x}}$ is the unit vector along the x-axis, and $\hat{\boldsymbol{t}}_\alpha = \hat{\boldsymbol{n}}_\alpha^{||}/|\hat{\boldsymbol{n}}_\alpha^{||}|$ with $\hat{\boldsymbol{n}}_\alpha^{||}$ denoting the projected swimming direction onto the x-y plane. The center of the probe sphere is located at $(x, y) = (0, 0)$. Following Fig. 5 in the main text, the plot settings in (a)-(f) are as follows: The panels present the distributions at $F_{ex} = 100$. The violet and dark-green lines correspond to $P(\hat{\theta}; x, y)$ $(x < 0)$ and $P(180° - \hat{\theta}; x, y)$ $(x > 0)$, respectively, calculated in the regions indicated by identical colored characters. The normalization factor $c(x, y)$ is determined so that the total area enclosed by these lines equals 1. The dotted lines guide the normal and tangential directions along the probe sphere.

In Fig. 5 in the main text, we present the orientation distribution of swimmers $P(\hat{\theta}; x, y)$ around the probe particle at $F_{ex} = 10$ and 100 with HIs. Here, Fig. S2 shows the results at $F_{ex} = 100$ without HIs.

For $x < 0$, a comparison of Fig. S2 with Fig. 5 reveals that the swimmers tend to move along the probe surface from the rear to the front more with HIs than without HIs. This behavior is attributable to HIs between the swimmers and the probe particle; at $F_{ex} = 100$ the flow field induced by the probe particle's motion is strong enough to guide the swimmers in the probe particle's moving direction. However, without HIs, there is a nearly equal distribution of swimmers moving from the rear to the front and in the opposite direction. On the other hand, for $x > 0$, in Figs. 5 and S2, we find that, in the regions labeled as (a) and (b), swimmers tend to face the probe particle more without HIs than with HIs; the swimmers are significantly scattered by hydrodynamic repulsions induced by the probe particle's movement. Also, in the regions indicated as (c)-(e), a similar distinction between with and without HIs is observed, although it is less pronounced.

D Derivation of the active stress

We here derive an expression for the local active stress tensor defined in a small subsystem denoted as K, with a volume V_K. Let us formally write the active force density due to the α-th swimmer as:

$$\nabla \cdot \overleftrightarrow{\boldsymbol{\sigma}}_{\alpha}^{act} = F_A \hat{\boldsymbol{n}}_\alpha \frac{\Psi_\alpha^{(b)}(\boldsymbol{r})}{\mathcal{V}_\alpha^{(b)}} - F_A \hat{\boldsymbol{n}}_\alpha \frac{\Psi_\alpha^{(f)}(\boldsymbol{r})}{\mathcal{V}_\alpha^{(f)}}, \tag{S17}$$

where the first term on the right-hand side represents the active force acting via the body-part region, included through the body force $\boldsymbol{f}_H$, and the second term represents that acting on the flagellum-part region, directly included in the Navier-Stokes equation, Eq. (5) in the main text. In this study, as described in Sec. 2 in the main text, the body and flagellum parts of the α-th swimmer are represented through the field variables $\Psi_\alpha^{(b)}(\boldsymbol{r})$ and $\Psi_\alpha^{(f)}(\boldsymbol{r})$, and whose explicit expressions are provided in Eqs. (1) and (2) in the main text, respectively. Furthermore, $\mathcal{V}_\alpha^{(b)}$ and $\mathcal{V}_\alpha^{(f)}$ represent the volumes of the body and flagellum, respectively. Here, $\overleftrightarrow{\boldsymbol{\sigma}}_{\alpha}^{act}$ is formally interpreted as the local active stress due to the α-th swimmer; its divergence yields the active force density as Eq. (S17). We integrate this expression by multiplying $\boldsymbol{r}$ over the subsystem K as:

$$\begin{aligned}
\int_K \mathrm{d}\boldsymbol{r} r_i \nabla_k \sigma_{\alpha,kj}^{act} &= \int_K \mathrm{d}\boldsymbol{r} \nabla_k [r_i \sigma_{\alpha,kj}^{act}] - \int_K \mathrm{d}\boldsymbol{r} \sigma_{\alpha,ij}^{act} \\
&= \int_{\partial K} \mathrm{d}S \hat{n}_k [r_i \sigma_{\alpha,kj}^{act}] - \int_K \mathrm{d}\boldsymbol{r} \sigma_{\alpha,ij}^{act} \\
&= F_A \int_K \mathrm{d}\boldsymbol{r} r_i \hat{n}_{\alpha,j} \left[\frac{\Psi_\alpha^{(b)}(\boldsymbol{r})}{\mathcal{V}_\alpha^{(b)}} - \frac{\Psi_\alpha^{(f)}(\boldsymbol{r})}{\mathcal{V}_\alpha^{(f)}} \right],
\end{aligned} \tag{S18}$$

where, for clarity, we express equations denoting coordinate components ($i, j, k = x, y, z$), and for simplicity, the summation convention is used. The first term on the right-hand side in the second line represents the surface integral over the boundary of the subsystem K. Here, $\hat{\boldsymbol{n}}$ represents the unit vector that is normal to and pointing outward from the enclosing surface ∂K, and $\mathrm{d}S$ denotes the surface area differential on ∂K. When the entire part of the α-th swimmer exists inside K, the active stress $\overleftrightarrow{\boldsymbol{\sigma}}_{\alpha}^{act}$ should be zero on ∂K, implying that the stress caused by the particle forces itself is local, affecting only the regions where the particles are located. Its propagation to distant regions occurs via the solvent in the form of the viscous stress. We finally obtain

$$\begin{aligned}
\int_K \mathrm{d}\boldsymbol{r} \overleftrightarrow{\boldsymbol{\sigma}}_{\alpha}^{act} &= -F_A \int_K \mathrm{d}\boldsymbol{r} \boldsymbol{r} \hat{\boldsymbol{n}}_\alpha \left[\frac{\Psi_\alpha^{(b)}(\boldsymbol{r})}{\mathcal{V}_\alpha^{(b)}} - \frac{\Psi_\alpha^{(f)}(\boldsymbol{r})}{\mathcal{V}_\alpha^{(f)}} \right] \\
&= -F_A \left(\boldsymbol{R}_\alpha^{(G)} - \boldsymbol{R}_\alpha^{(CF)} \right) \hat{\boldsymbol{n}}_\alpha \\
&= -F_A \ell_0 \hat{\boldsymbol{n}}_\alpha \hat{\boldsymbol{n}}_\alpha.
\end{aligned} \tag{S19}$$

By setting $(1/V_K) \int_K \mathrm{d}\boldsymbol{r} \overleftrightarrow{\boldsymbol{\sigma}}_{\alpha}^{act}$ as a contribution from the α-th swimmer, we define the average active stress in a small subsystem K as Eq. (34) in the main text. This derivation can also be used to calculate the particle stress, and the obtained expression corresponds with that derived through the method detailed in the reference[4], which is based on the fundamental stress definition.

It is worth to note the following. Equation (S19) is ideally derived for situations where particulate forces are modeled as point forces. However, in the present study, particles are not represented as points but as finite regions defined by $\Psi_\alpha^{(b)}$ and $\Psi_\alpha^{(f)}$, meaning that the active forces are no longer regarded as point forces. For such a case, in Eq. (S19), these $\Psi_\alpha^{(b)}$ and $\Psi_\alpha^{(f)}$ likely cross the boundary of the given hypothetical subspace, over which the average is taken. This situation may complicate how we split the stress between different adjacent subspaces. Nevertheless, when focusing on average stresses rather than instantaneous stresses, the distinction between modeling particles as points or regions does not matter. Because the average stress is calculated through a smooth positional distribution function, the difference between the two cases does not significantly affect the overall result.

Notes and references

1 H. Hayano and A. Furukawa, Phys. Rev. Research **4**, 043091 (2022).

2 J. J. Molina, K. Otomura, H. Shiba, H. Kobayashi, M. Sano, and R. Yamamoto, J. Fluid Mech. **792**, 590 (2016).

3 R. Yamamoto, J. J. Molina, and Y. Nakayama, Soft Matter **17**, 4226 (2021).

4 M. Doi and S. F. Edwards, *The Theory of Polymer Dynamics*, (Clarendon Press, Oxford, 1988).